Annals of Botany **104**: 1373–1387, 2009
doi:10.1093/aob/mcp255, available online at www.aob.oxfordjournals.org

ANNALS OF BOTANY
Founded 1887

The role of callose in guard-cell wall differentiation and stomatal pore formation in the fern *Asplenium nidus*

P. Apostolakos, P. Livanos, T. L. Nikolakopoulou and B. Galatis*

Department of Botany, Faculty of Biology, University of Athens, Athens 15784, Greece

Received: 15 July 2009 Returned for revision: 18 August 2009 Accepted: 10 September 2009 Published electronically: 13 October 2009

• *Background and Aims* The pattern of callose deposition was followed in developing stomata of the fern *Asplenium nidus* to investigate the role of this polysaccharide in guard cell (GC) wall differentiation and stomatal pore formation.
• *Methods* Callose was localized by aniline blue staining and immunolabelling using an antibody against (1 → 3)-β-D-glucan. The study was carried out in stomata of untreated material as well as of material treated with: (1) 2-deoxy-D-glucose (2-DDG) or tunicamycin, which inhibit callose synthesis; (2) coumarin or 2,6-dichlorobenzonitrile (dichlobenil), which block cellulose synthesis; (3) cyclopiazonic acid (CPA), which disturbs cytoplasmic Ca^{2+} homeostasis; and (d) cytochalasin B or oryzalin, which disintegrate actin filaments and microtubules, respectively.
• *Results* In post-cytokinetic stomata significant amounts of callose persisted in the nascent ventral wall. Callose then began degrading from the mid-region of the ventral wall towards its periphery, a process which kept pace with the formation of an 'internal stomatal pore' by local separation of the partner plasmalemmata. In differentiating GCs, callose was consistently localized in the developing cell-wall thickenings. In 2-DDG-, tunicamycin- and CPA-affected stomata, callose deposition and internal stomatal pore formation were inhibited. The affected ventral walls and GC wall thickenings contained membranous elements. Stomata recovering from the above treatments formed a stomatal pore by a mechanism different from that in untreated stomata. After coumarin or dichlobenil treatment, callose was retained in the nascent ventral wall for longer than in control stomata, while internal stomatal pore formation was blocked. Actin filament disintegration inhibited internal stomatal pore formation, without any effect on callose deposition.
• *Conclusions* In *A. nidus* stomata the time and pattern of callose deposition and degradation play an essential role in internal stomatal pore formation, and callose participates in deposition of the local GC wall thickenings.

Key words: *Asplenium nidus*, callose, stomatal pore formation, guard cell wall differentiation.

INTRODUCTION

Stomata are highly differentiated structures that regulate the gaseous exchange between the aerial plant organs and external environment, and play a critical role in plant water status and photosynthetic performance (Willmer and Fricker, 1996). Extensive research work has been carried out on stomatal development and differentiation (for literature see Sack, 1987; Galatis and Apostolakos, 2004). One of the main stages in stomatal development is the formation of an epidermal intercellular space (the stomatal pore) between the guard cells (GCs), which brings the internal plant tissues into contact with the external environment (Fig. 1A). In angiosperms, stomatal pore formation is a phenomenon concomitant with GC morphogenesis, during which the middle regions of the adjacent ventral walls separate (Galatis and Apostolakos, 2004; see also Sack, 1987; Willmer and Fricker, 1996). In these plants, local ventral wall separation begins at the junction of the middle regions of the ventral wall with the periclinal walls and proceeds inwards (Fig. 1B, C; see also Sack, 1987; Galatis and Apostolakos, 2004). In contrast, an extraordinary mechanism of stomatal pore formation is found in Polypodiales ferns. In these plants, the stomatal pore appears first as an intercellular space at the centre of the post-cytokinetic ventral wall ('internal stomatal pore'; Fig. 1D), which gradually expands towards the external and internal periclinal GC walls. At an advanced stage of GC differentiation, the periclinal walls over the 'internal stomatal pore' are disrupted and the stomatal pore is completed (Fig. 1E; see Galatis *et al.*, 1983; Apostolakos and Galatis, 1998, 1999; Zachariadis *et al.*, 1998).

The differentiating fern stomata are also characterized by the deposition of significant quantities of callose in their walls (see below). Callose is an amorphous (1 → 3)-β-D-glucan that is synthesized by callose synthase, an enzyme localized in the plasmalemma (Verma and Hong, 2001; Bulone, 2007). It represents a highly dynamic cell-wall component, usually of temporal character, which is implicated in a wide variety of cell activities (Stone and Clarke, 1992). The presence of callose in developing angiosperm stomata has been correlated with stomatal pore formation (see review by Galatis and Apostolakos, 2004). In the fern *Asplenium nidus*, this glucan is deposited at particular regions of the differentiating ventral and periclinal GC walls (Apostolakos and Galatis, 1998, 1999). Comparable observations have also been made in stomata of other ferns (Peterson *et al.*, 1975; Peterson and Hambleton, 1978; Waterkeyn and Bienfait, 1979).

* For correspondence. E-mail bgalatis@biol.uoa.gr

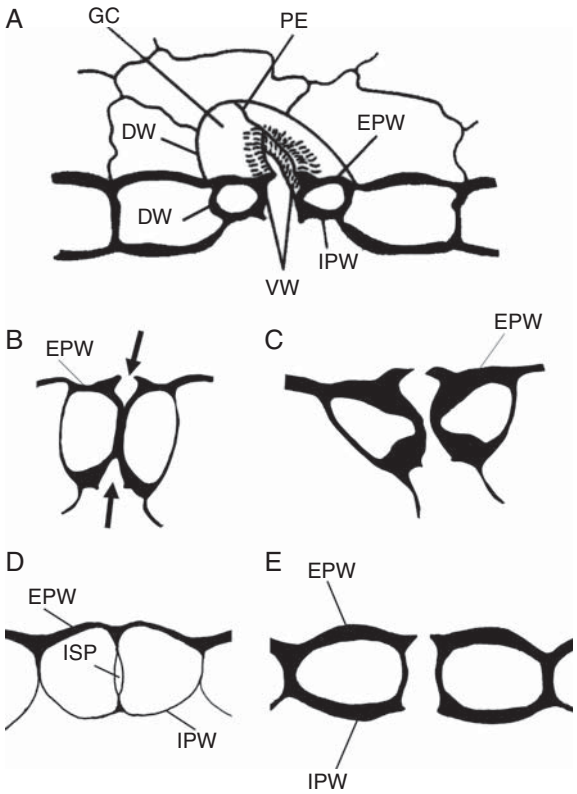

FIG. 1. (A) Diagrammatic representation of an elliptical stoma. (B–E) Diagram to show the process of stomatal pore formation in angiosperms (B, C) and some Polypodiales ferns (D, E). The arrows in (B) indicate the forming stomatal pore. Abbreviations: DW, dorsal wall; EPW, external periclinal wall; GC, guard cell; IPW, internal periclinal wall; ISP, internal stomatal pore; PE, polar ventral wall end; VW, ventral wall.

Recent work has revealed that in the periclinal walls of *A. nidus* stomata callose is deposited in the form of fibrils organized in radial arrays focused on the stomatal pore region, similar to those of cellulose microfibrils in the same walls and the underlying microtubules. The latter seem to control the pattern of deposition of these radial callose fibril arrays (Apostolakos *et al.*, 2009).

The present work attempts to investigate the probable role of callose in stomatal pore formation and GC wall differentiation in Polypodiales ferns by detailed examination of: (1) the pattern of deposition/degradation of callose in differentiating GCs of *A. nidus*, particularly during stomatal pore formation, and (2) the effects of substances that inhibit or induce callose formation on stomatal development. As the deposition of radial callose fibril arrays in *A. nidus* stomata seems to be controlled by microtubules (Apostolakos *et al.*, 2009), it was also examined whether substances disintegrating microtubules and actin filaments affect the pattern of callose deposition in developing stomata.

MATERIALS AND METHODS

Callose localization

Callose in living *Asplenium nidus* L. stomata was localized using aniline blue staining (O'Brien and McCully, 1981). Callose was also labelled in fixed free-hand and semi-thin sections using a monoclonal antibody against $(1 \rightarrow 3)$-β-D-glucans (Meikle *et al.*, 1991; Ferguson *et al.*, 1998).

Treatments

The role of callose in stomatal development was further investigated by treatment of developing *A. nidus* leaves with:

(1) The inhibitors of callose synthesis 2-deoxy-D-glucose (2-DDG; Jaffe and Leopold, 1984) and tunicamycin (Škalamera and Heath, 1996), substances that may also affect cellulose microfibril synthesis (Quader, 1984).
(2) The inhibitors of cellulose synthesis coumarin and 2,6-dichlorobenzonitrile (dichlobenil; Montezinos and Delmer, 1980; Vaughn *et al.*, 1996; Sabba *et al.*, 1999). Inhibition of cellulose synthesis by the above substances promotes callose synthesis (Vaughn *et al.*, 1996; DeBolt *et al.*, 2007). These treatments, among others, allow discrimination of the disturbances in stomatal development, which are induced by callose synthesis inhibitors from those caused by inhibition of cellulose synthesis.
(3) Cyclopiazonic acid (CPA), which disturbs cytoplasmic Ca^{2+} homeostasis, affecting the function of Ca^{2+} pumps in endoplasmic reticulum (Quader and Bechtler, 1996), as it is known that Ca^{2+} controls callose deposition (Verma and Hong, 2001).

The role of the cytoskeleton in callose deposition and stomatal pore formation was investigated by treatment with oryzalin and cytochalasin B, which disintegrate microtubules and actin filaments, respectively.

Leaves of *A. nidus* were treated with: (1) 500 μM or 1 mM 2-DDG for 48–72 h, (2) 12 μM tunicamycin for 48–72 h, (2) 500 μM coumarin for 72 h, (4) 100 μM dichlobenil for 12–72 h, (5) 25 μM CPA for 12–48 h, (6) 100 μM cytochalasin B for 48–72 h or (g) 50 μM oryzalin for 72 h. All substances were obtained from Sigma (St Louis, MO, USA) except for CPA and oryzalin, which were kindly provided by Dr H. Quader (Biocenter Klein Flottbek, University of Hamburg). They were dissolved in water, except for CPA, which was dissolved in Tris/maleate buffer (5 mM), at pH 5·0. The water solutions of tunicamycin, coumarin, dichlobenil and cytochalasin B were prepared from stock solutions of these substances in dimethyl sulfoxide (DMSO), while that of oryzalin was prepared from a stock solution in acetone. The very low final concentrations of DMSO or acetone in the treatment solutions did not induce side-effects (Panteris *et al.*, 2006).

Treatments were carried at room temperature, except for those with tunicamycin, which were applied in the dark at 25 ± 1 °C. In all cases, apical leaf regions were placed on cotton moistened with the drug solutions. Apical leaf regions placed on cotton moistened with distilled water were used as controls.

In some experiments, apical leaf regions were placed in cotton moistened with either 500 μM 2-DDG or 12 μM tunicamycin for 5 d. They were then placed on cotton wetted with distilled water for 7 d at room temperature (control conditions).

Transmission electron microscopy (TEM)

Small pieces of untreated and treated leaves were prepared for light microscopy and TEM examination. Material was pre-fixed with 3 % (v/v) glutaraldehyde plus 1 % (w/v) tannic acid in 50 mM sodium cacodylate buffer, pH 6·8, for 2 h at room temperature, post-fixed with 1 % (w/v) osmium tetroxide in the same buffer for 12 h at 4 °C, dehydrated in an acetone series and embedded in Spurr's resin. Semi-thin sections were stained with 1 % (w/v) toluidine blue made in 1 % (w/v) borax solution and were examined with a Zeiss Axioplan microscope equipped with a Zeiss Axiocam MRc5 digital camera. Thin sections were stained with uranyl acetate and lead citrate and examined with a Philips 300 or Philips 420 transmission electron microscope.

Fluorescence microscopy

Callose identification. For callose immunolabelling in semi-thin sections, small leaf pieces were fixed in 2 % (w/v) paraformaldehyde and 0·1 % (v/v) glutaraldehyde in PEM (50 mM PIPES, 5 mM EGTA, 10 mM $MgSO_4$), pH 6·8, at 4 °C for 1·5 h. After fixation, the specimens were washed in the same buffer and dehydrated in a graded ethanol series (10–90 %) diluted in distilled water and in absolute ethanol three times, for 30 min (each step) at 0 °C. They were post-fixed with 0·25 % (w/v) osmium tetroxide added to the 30 % ethanol step for 2 h. They were then infiltrated with LR White (LRW) acrylic resin diluted in ethanol, in 10 % steps to 100 % (1 h in each), at 4 °C and finally with pure resin overnight. The specimens were embedded in gelatine capsules filled with LRW resin and polymerized at 60 °C for 48 h.

Semi-thin sections of material embedded in LRW resin were transferred to glass slides and blocked with 5 % (w/v) bovine serum albumin (BSA) in phosphate-buffered saline (PBS) for 5 h. After washing with PBS, mouse anti-(1 → 3)-β-D-glucan monoclonal antibody (Biosuplies, Australia Ltd) diluted 1 : 40 in PBS containing 2 % (w/v) BSA was applied overnight at room temperature. After rinsing with PBS and blocking again with 2 % (w/v) BSA in PBS, the sections were incubated for 1 h at 37 °C in fluorescein isothiocyanate (FITC) anti-mouse IgG (Sigma) diluted 1 : 40 in PBS containing 2 % (w/v) BSA. Following rinsing with PBS, the sections were mounted on glass slides using an anti-fade mounting medium containing *p*-phenylenediamine.

Hand-made leaf sections of control and treated material were fixed in 8 % (w/v) paraformaldehyde in PEM, pH 6·8, for 45 min at room temperature, washed three times with PEM for 15 min and treated with 1 % (w/v) cellulase (Onozuka) in PEM for 30 min. After washing with PEM, the sections were extracted with 3 % (v/v) Triton X-100 and 5 % (v/v) DMSO in PBS for 1 h and then transferred to PBS containing 3 % (w/v) BSA for 1 h. Sections were incubated overnight with the same anti-callose antibody and rinsed with PBS three times for 15 min. They were then transferred to PBS containing 2 % (w/v) BSA and incubated in FITC-IgG as above, washed with PBS and finally covered with anti-fade solution.

Callose was also localized in hand-made sections of living material stained with 0·05 % aniline blue (Sigma, C.I. 42725) in 0·07 M K_2HPO_4 buffer, pH 8·5 (Apostolakos and Galatis, 1998, 1999).

The cell-wall polysaccharides, other than callose, were localized in semi-thin sections via the Periodic acid–Schiff (PAS) method (Roland, 1978) or by staining with 0·001 % (w/v) calcofluor white M2R (Tinopal LPW; Sigma) in PBS for 10 min.

The semi-thin and hand-made sections were examined with a Zeiss Axioplan microscope equipped with a UV source, proper filters (one with exciter G 365 and barrier LP 420 and another with exciter BP 450–490 and barrier BP 515–565) and a Zeiss Axiocam MRc5 digital camera as well as with a confocal laser scanning microscope (Leica TCS-SP5, Microsystems, Bensheim, Germany). All samples were checked for UV autofluorescence.

Actin filament and microtubule localization. Microtubules and actin filaments were visualized following the procedures described by Apostolakos and Galatis (1998, 1999) and Panteris *et al.* (2007). Briefly, for microtubule immunolabelling the specimens were initially fixed with paraformaldehyde, the cell walls were partially digested with enzymes and they were successively incubated with the monoclonal rat anti-tubulin antibody and FITC anti-rat IgG. For actin filament localization the material was treated first with *m*-maleimidobenzoyl-*N*-hydroxysuccinimide ester for actin filament stabilization, then fixed with paraformaldehyde and finally stained with Alexa-Fluor 568 phalloidin (Invitrogen). All specimens were examined with a Zeiss Axioplan microscope and a confocal laser scanning microscope (Leica TCS-4D, Microsystems).

RESULTS

General remarks

The *Asplenium* stomata have kidney-shaped GCs (Fig. 2A). The anticlinal wall separating the GCs, where the stomatal pore forms, is the ventral wall while the anticlinal walls shared with the surrounding epidermal cells are the dorsal walls (Fig. 2A). The GC walls parallel to the leaf surface are the periclinal walls. The ventral wall regions between the stomatal pore and the ventral wall edges are defined as polar ventral wall ends (Fig. 2A; see also Fig. 1A).

Both aniline blue staining and immunolabelling with the monoclonal (1 → 3)-β-D-glucan antibody applied to localize callose gave reliable, almost identical results (Fig. 3B; cf. Fig. 4A; see also Apostolakos *et al.*, 2009). Aniline-blue-stained callose was detected using the filter with barrier LP 420, while callose immunofluorescence was detected using the filter with barrier BP 515–565. To distinguish callose fluorescence from the GC wall autofluorescence, unstained material was examined with a fluorescence microscope using the above filters. Autofluorescence displayed the polar ends of the ventral wall of mature stomata only (Fig. 2B, C; see also Apostolakos *et al.*, 2009). This is clearly distinguished from callose fluorescence (Fig. 2C; cf. Fig. 3H).

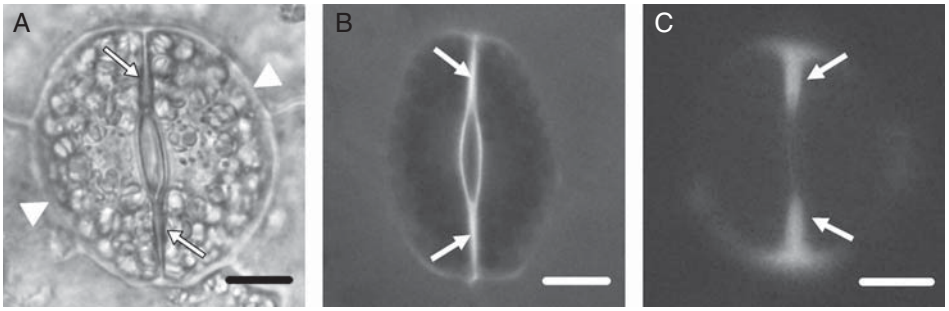

FIG. 2. (A) Light micrograph of a control living stoma. The arrows mark the ventral wall and the arrowheads the dorsal walls. Scale bar = 10 μm. (B, C) Epifluorescence microscope images of unstained control stomata showing the guard cell wall regions emitting autofluorescence. (B) Stoma observed under the filter with exciter G 365 and barrier LP 420. (C) Stoma observed under the filter with exciter BP 450–490 and barrier BP 515–565. The arrows point to cell-wall regions exhibiting UV autofluorescence. Scale bars = 10 μm.

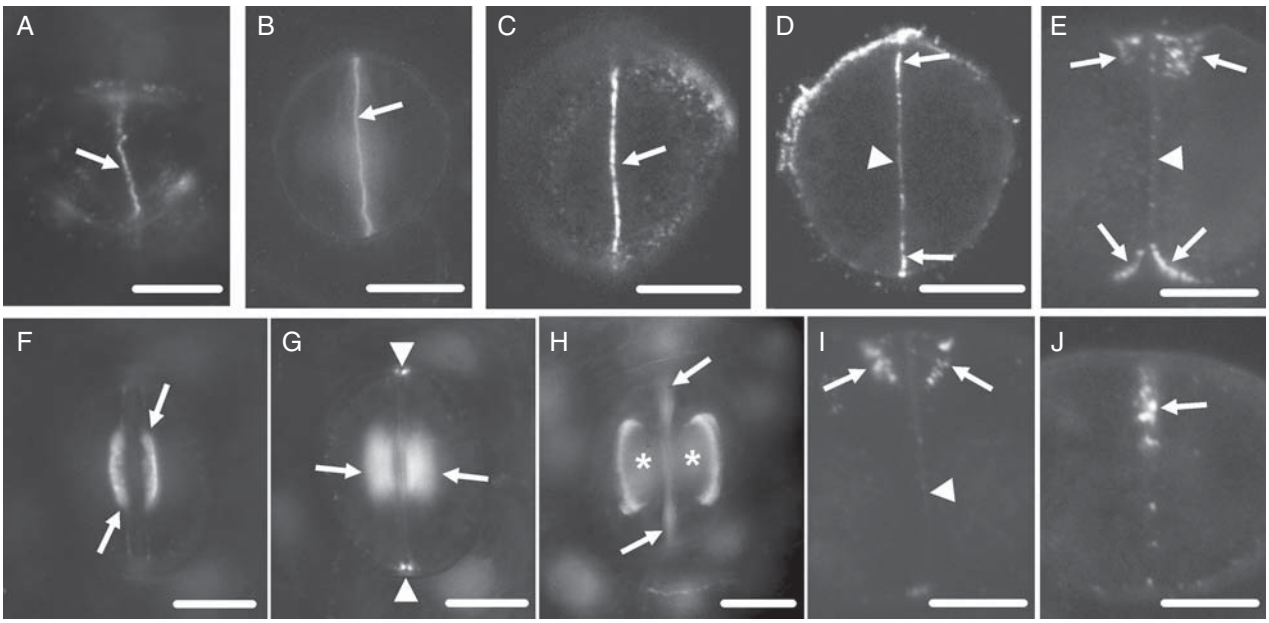

FIG. 3. Callose localization in developing control stomata after immunolabelling (A, C–J) or aniline blue staining (B). Scale bars = 10 μm. (A) Cytokinetic guard cell mother cell. The arrow indicates the cell plate. (B) Post-cytokinetic stoma. The nascent ventral wall (arrow) exhibits intense callose fluorescence. (C, D) Single CLSM sections through the junction of the ventral wall with the external periclinal walls (C) and a median plane (D) of a stoma in which the internal stomatal pore has been initiated. The margins of the ventral wall (arrows in C and D) exhibit intense callose fluorescence and a less intense one at its median region (arrowhead in D). (E) Median transverse semi-thin section of a stoma, in which stomatal pore formation and wall thickening deposition have started. Wall thickenings containing callose emerge at the junctions of the ventral wall with the periclinal walls (arrows; cf. Fig. 5B). The rest of the ventral wall (arrowhead) lacks callose. (F, G) Optical sections through a surface (F) and an inner plane (G) of a stoma at an early stage of wall thickening. Callose impregnates the wall thickenings at the stomatal pore region (arrows in F and G) and at the junctions of the ventral wall with the dorsal walls (arrowheads in G). (H) Stoma at a more advanced stage of differentiation than that shown in F and G. Callose is detected at the margins of the wall thickenings (asterisks) at the stomatal pore region. The arrows point to ventral wall regions displaying autofluorescence (cf. Fig. 2C). (I) Median transverse semi-thin section of a stoma at the same differentiation stage as that of the stoma shown in (H). Callose is located at the margins of the wall thickenings (arrows). The rest of the ventral wall lacks callose (arrowhead). (J) Transverse semi-thin section of a ventral wall polar end (see Fig. 1A). Callose (arrow) is deposited at the wall thickening developing in this area (cf. Fig. 5E).

Untreated stomata: pattern of callose deposition/degradation and stomatal pore initiation

In cytokinetic GC mother cells, callose was deposited along the whole surface of the developing and recently completed cell plate (Fig. 3A). Intense callose fluorescence was also emitted by the post-cytokinetic ventral walls, which persisted for a relatively long time in the nascent ventral walls (Figs 3B and 4A).

In young stomata, i.e. those at the stage of initiation of the stomatal pore and local wall deposition (Apostolakos and Galatis, 1998, 1999), callose degradation commenced at the centre of the ventral wall and proceeded towards its periphery (Figs 3C, D and 4B–F). Confocal laser scanning microscopy (CLSM) showed that the pattern of post-cytokinetic callose degradation differs between nascent ventral walls and nascent ordinary protodermal cell walls. In the latter, callose degradation is centripetal, i.e. commences from their periphery and proceeds internally (Fig. 4A–F).

Later, callose was found at the junctions of the ventral wall with the periclinal (Figs 3C and 4B, E) and dorsal walls

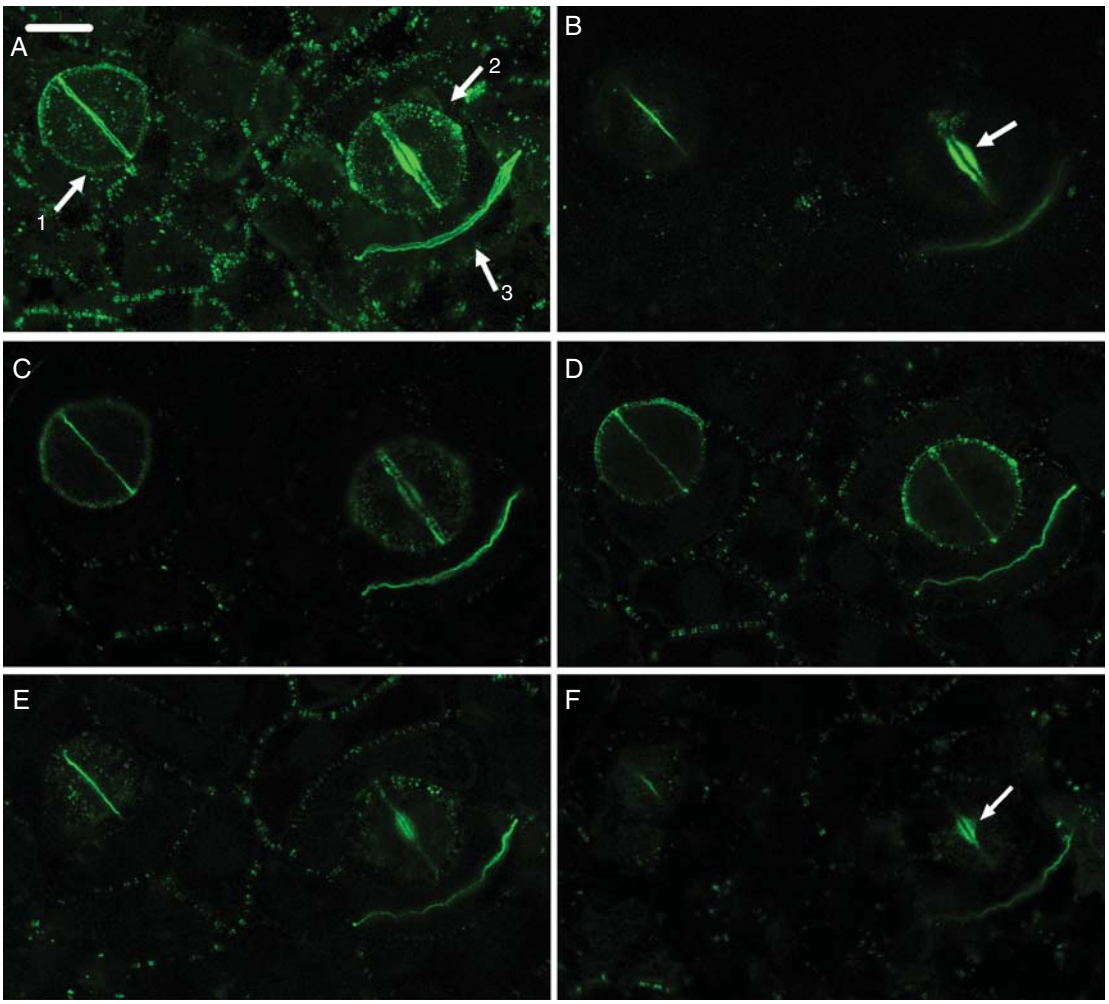

FIG. 4. (A–F) Paradermal CLSM view of control stomata at an early (arrow 1 in A) and a more advanced (arrow 2 in A) stage of differentiation and a dividing ordinary protodermal cell (arrow 3 in A), after callose immunolocalization. In stoma No. 1 the internal stomatal pore has been initiated, while in stoma No. 2 the deposition of wall thickening has started. (A) Figure produced by projection of 51 CLSM sections. (B–F) Figures produced by projection of four consecutive CLSM sections each. (B) Plane close to the external periclinal walls. (C, D) Median planes. (E, F) Planes close to the internal periclinal walls. For determination of the external and internal periclinal walls see Fig. 1A. The ventral wall emits intense callose fluorescence at regions close to the periclinal walls (B, E), while the nascent daughter wall of the protodermal cell emits intense callose fluorescence at central regions (C, D). The arrows in (B) and (F) indicate the wall thickenings at the stomatal pore region. Scale bar = 10 μm.

(Figs 3G and 4D) and in the initiating wall thickenings at the junctions of the middle of the ventral wall with the periclinal walls (Figs 3E, F and 4B, F; see also Fig. 5B). The periclinal walls displayed radial fibril callose arrays converging on the site of the future stomatal pore (Apostolakos *et al.*, 2009). At this stage, the stomatal pore has already been initiated 'internally'. It represents an isolated intercellular space at mid depth of the ventral wall (Fig. 5A, B). The absence of callose from the walls lining the newly formed internal stomatal pore shows that it appears after callose degradation at the mid-region of the ventral wall (Fig. 3D, E). Given the similarity between GC shape and local wall thickenings, it can be concluded that the stomata shown in Fig. 3D and E are at the same developmental stage as that of those illustrated in Fig. 5A and B, respectively.

The differentiating stomata, in which stomatal pore formation was advanced, displayed distinct local wall thickenings at the junctions of the middle of the ventral wall with the periclinal walls (Fig. 5C) and at those of the polar ventral wall ends with the external periclinal wall (Fig. 5E). Along the middle lamella of the ventral wall thickenings the fore- and rear-chambers of the stomatal pore developed and became connected with the internal stomatal pore (Fig. 5C, D; see also Apostolakos and Galatis, 1998). Parallel with stomatal pore formation, the whole central region of the periclinal GC walls was locally thickened. In those stomata, callose appeared in the junctions of the ventral wall with the rest of the walls, in the margins of the GC wall thickenings around the stomatal pore (Fig. 3H, I) and in the thickenings deposited at the polar ventral wall ends (Fig. 3J).

Stomata treated with callose synthesis inhibitors: the absence of callose inhibits stomatal pore formation

In 2-DDG-treated leaves, callose deposition was inhibited in cell plates of the GC mother cells and in the nascent ventral

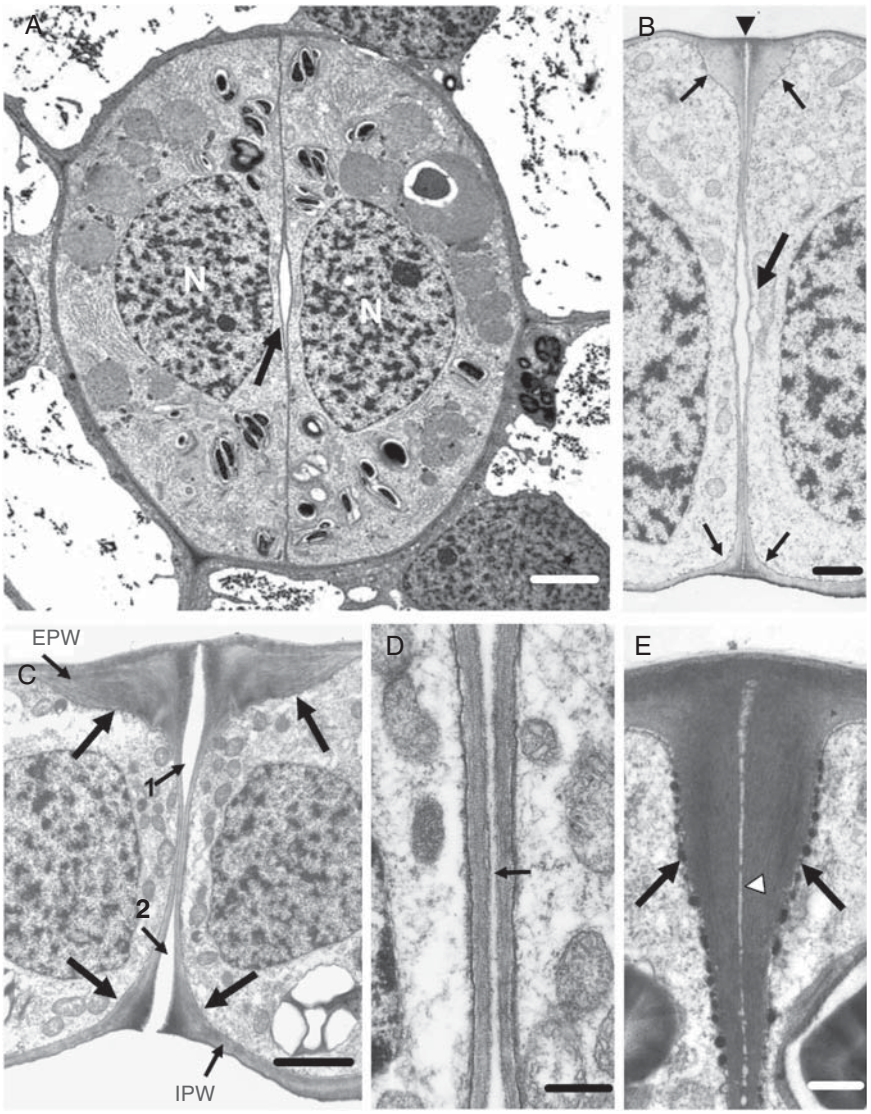

FIG. 5. Untreated stomata as appear in TEM. (A) Median paradermal section of a stoma in which the internal stomatal pore (arrow) has been initiated. N, nucleus. Scale bar = 2 μm. (B) Median transverse section of a stoma at a differentiation stage similar to that of the stoma shown in (A). The large arrow points to the internal stomatal pore, while the small arrows point to the wall thickenings deposited at the external and internal stomatal pore region. The arrowhead marks the initiating fore-chamber of the stomatal pore. Scale bar = 1 μm. (C) Median transverse section of a stoma at a later stage of differentiation than that of the stoma shown in (B). Large arrows show the wall thickenings at the stomatal pore region, whereas the small arrows 1 and 2 show the fore- and rear-pore chamber, respectively. The periclinal wall covering the rear-pore chamber has been disrupted. EPW, external periclinal wall; IPW, internal periclinal wall. Scale bar = 2 μm. (D) Median ventral wall region of the stoma shown in (C) at higher magnification. The stomatal pore (arrow) appears as a slit between the adjacent ventral walls. Scale bar = 500 nm. (E) Transverse view of a polar ventral wall end. For determination of the polar ventral wall end see Fig. 1A. The arrows mark the wall thickenings, while the arrowhead marks the middle lamella. Scale bar = 500 nm.

walls (Fig. 6A, B; cf. Fig. 3B). The affected differentiating stomata exhibited weak callose labelling in the wall thickenings at the stomatal pore region (Fig. 6C; cf. Figs 3F and 4B) and the polar ventral wall ends.

TEM examination of young treated stomata showed that the 2-DDG treatment blocks internal stomatal pore formation (Fig. 7A; cf. Fig. 5B). The median ventral wall region was abnormally thickened, electron-transparent and contained membranous elements (Fig. 7A, B). The wall thickenings of the affected stomata were also electron-transparent and enclosed membranous elements (Fig. 7C). These membranous elements cannot be considered as artefacts of chemical fixation, because they were not observed in untreated stomata (Fig. 5B, C), which had followed the same fixation procedure. The aberrant ventral walls of the affected stomata fluoresced intensely after calcofluor staining (Fig. 7A, inset), indicating that polysaccharides, other than callose, have been deposited in them.

Considering that the cytoskeleton is implicated in the mechanism of the internal stomatal pore formation (Apostolakos and Galatis, 1998), microtubule and actin filament organization was examined in 2-DDG-affected stomata. The pattern of their organization was not altered. As in untreated stomata, the microtubules were arrayed in distinct bands

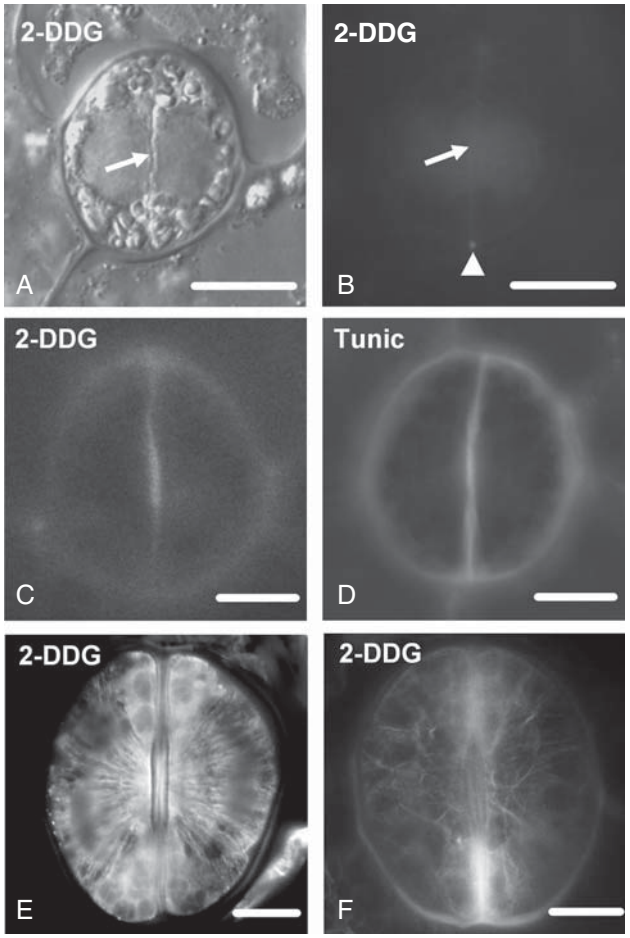

FIG. 6. (A) Differential interference contrast optical view of a post-cytokinetic 2-DDG-affected stoma. The arrow shows the nascent ventral wall. (B) The stoma after callose localization with aniline blue staining. The nascent ventral wall (arrow) does not display callose fluorescence (cf. Fig. 3B). Weak callose fluorescence is emitted by the junctions of the ventral wall with the dorsal walls (arrowhead). Treatment: 1 mM 2-DDG for 48 h. Scale bar = 10 μm. (C, D) Callose localization after aniline blue staining in a 2-DDG- (C) and a tunicamycin-affected (D) differentiating stoma. Treatments: (C) 1 mM 2-DDG for 48 h; (D) 24 μM tunicamycin for 48 h. Scale bars = 10 μm. (E, F) Microtubule immunolabelling (E) and actin filament staining (F) with Alexa Fluor 568 phalloidin in 2-DDG-affected differentiating stomata. Treatment: 500 μM 2-DDG for 72 h. Scale bars = 10 μm.

lining anticlinally both the sides of the ventral wall at the stomatal pore region and in radial systems beneath the periclinal walls (Fig. 6E). Most of the actin filaments underlying the periclinal walls in the differentiating affected stomata terminated at the stomatal pore region (Fig. 6F).

The effects of tunicamycin on *A. nidus* stomata were similar to those produced by 2-DDG. The developing stomata lacked callose (Fig. 6D; cf. Fig. 3F, H), and there was no internal stomatal pore formation (Fig. 7D; cf. Fig. 5B). The affected ventral wall was locally thickened, electron-transparent and included membranous elements (Fig. 7D, E). Calcofluor staining showed that these ventral walls contained polysaccharides other than callose (Fig. 7D, inset). The atypical cell-wall thickenings of the tunicamycin-affected stomata also possessed membranous elements (Fig. 7F).

Stomatal pore formation in 2-DDG- or tunicamycin-affected stomata did not begin even after 5 d of treatment (Fig. 8A). However, when they were transferred in control conditions, stomatal pore formation started by the simultaneous detachment of the adjacent ventral walls at the levels of the external and internal periclinal walls, proceeding inwards (Fig. 8B). Figure 8C–E illustrates stomata allowed to recover for 7 d, after 5 d of 2-DDG (Fig. 8C, D) or tunicamycin (Fig. 8E) treatment. In the young stoma shown in the inset to Fig. 8C, the detachment of the ventral wall partners has not started. However, along the whole depth of the ventral wall a modified middle lamella can be observed, which contains a homogeneous, lipophilic, cuticular-like material (Fig. 8C) that was positive to Sudan black B (see Supplementary Data Fig. S1A, available online). In the stoma shown in the inset to Fig. 8D, the fore- and rear-pore chamber formation has started (arrows). The modified middle lamella of the rest of the unseparated, ventral wall regions displayed lipophilic material (Fig. 8D).

In the stoma illustrated in the inset to Fig. 8E, the stomatal pore is at a final stage of formation. The ventral walls remain attached only in their central region, while the periclinal wall over the rear-pore chamber has been disrupted (Fig. 8E, inset). The middle lamella of the central, unseparated, ventral wall region possesses lipophilic material (Fig. 8E). A similar material has not been observed in the separated ventral wall regions of the untreated stomata (Fig. 5D). The arrow in Fig. 8E indicates a bridge of wall material connecting the adjacent ventral walls.

Stomata treated with cellulose synthesis inhibitors: inhibition of callose degradation blocks stomatal pore formation

The dichlobenil- or coumarin-affected stomata displayed more extensive callose deposition than controls (Fig. 9A, B; cf. Fig. 3F, H, respectively). Abundant callose was present along the whole surface of the nascent ventral walls (Fig. 9C, D). In contrast to the nascent ventral walls of control stomata, callose degradation was inhibited in dichobenil- or coumarin-affected stomata. The median (Fig. 9D) and marginal regions (Fig. 9C) of the nascent ventral wall of a dichlobenil-affected stoma emitted intense callose fluorescence. In contrast, in control stomata of the same stage of differentiation, the central ventral wall regions were devoid of callose (Figs 3D and 4D).

TEM examination revealed that the dichlobenil- or coumarin-affected GC walls were extensively disturbed. The ventral wall in the young affected stoma shown in the inset to Fig. 9E is very thin and lacks fibrillar material, thickenings and membranous elements (Fig. 9E). Notably, in the dichlobenil- or coumarin-affected stomata the internal stomatal pore formation has been blocked (Fig. 9E; cf. Fig. 5B).

Stomata treated with anti-cytoskeletal drugs: cytoskeleton disintegration interferes with stomatal pore formation

The data presented above revealed a consistent callose deposition in developing GC wall thickenings, the morphogenesis of which is microtubule-dependent (Galatis and Apostolakos, 2004). In *A. nidus* and other polypodiaceous fern stomata,

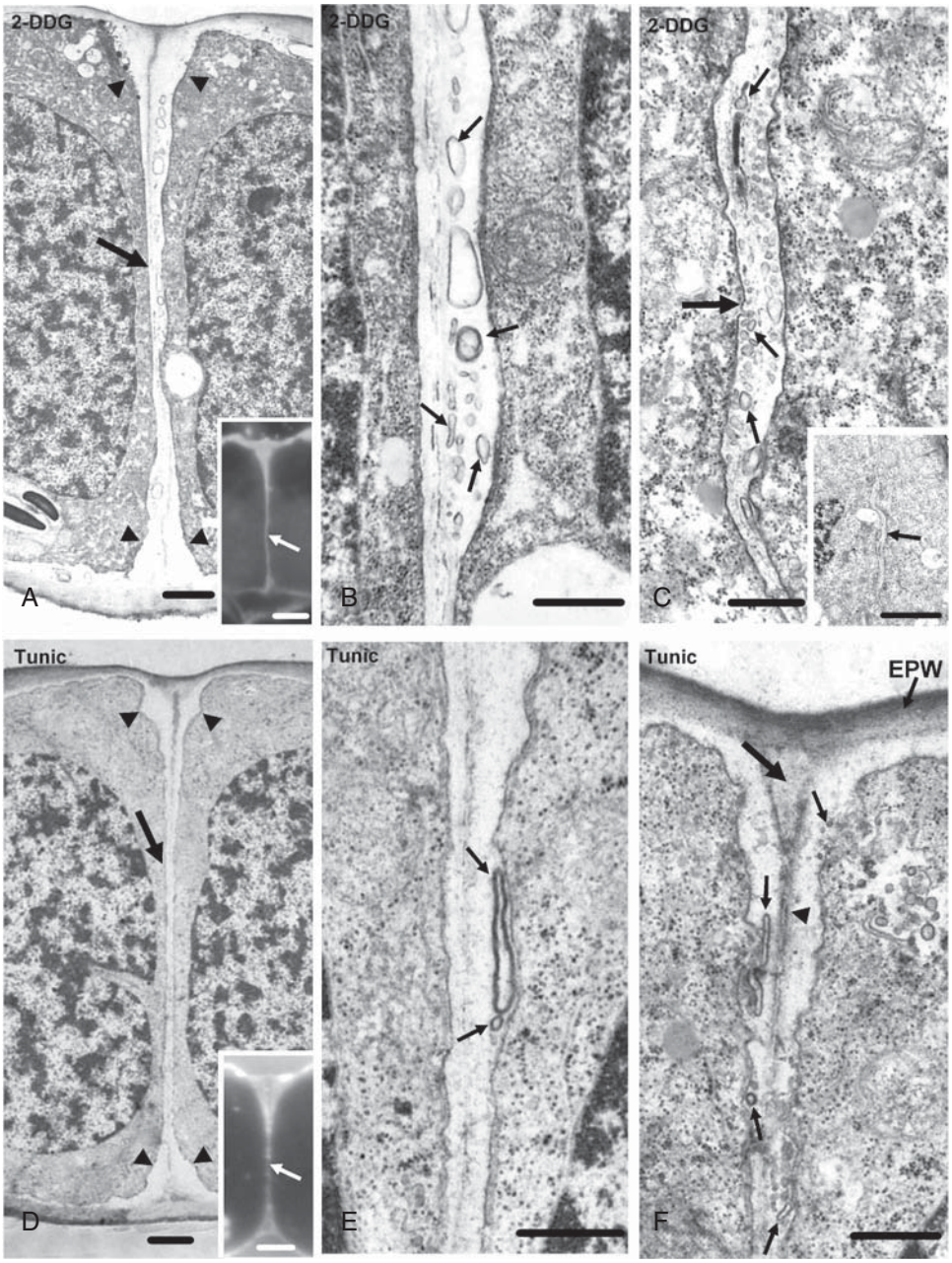

FIG. 7. TEM micrographs of stomata treated with callose synthesis inhibitors, showing the inhibition of internal stomatal pore formation. Treatments: (A–C) 1 mM 2-DDG for 48 h; (D–F) 12 μM tunicamycin for 48 h. (A) Median transverse section of a 2-DDG-affected stoma, which is at a stage of differentiation similar to that of the stomata shown in Fig. 5A and B. The arrow points to the aberrant ventral wall and the arrowheads to its atypical wall thickenings. Inset: median transverse semi-thin section of a 2-DDG-affected stoma at the same stage of differentiation as that of the stoma illustrated in (A), after calcofluor staining. The ventral wall (arrow) fluoresces along its whole depth. Scale bars: (A) = 1 μm; inset = 5 μm. (B) Higher magnification of the median ventral wall region of the stoma shown in (A). The apoplast contains numerous membranous elements (arrows). Scale bar = 500 nm. (C) Paradermal section through the wall thickening (large arrow) deposited at the junction of the middle of the ventral wall with the periclinal walls in a 2-DDG-affected stoma. Note the numerous membranous elements (small arrows) in the wall thickening. Inset: the arrow points to the wall thickening shown in (C) at higher magnification. Scale bars: (C) = 500 nm; inset = 5 μm. (D) Median transverse section of a tunicamycin-affected stoma at a stage of differentiation similar to that of the stomata illustrated in Fig. 5A and B. The arrow shows the ventral wall and the arrowheads the wall thickenings at their junctions with the periclinal walls. Inset: median transverse semi-thin section of a tunicamycin-affected stoma at a stage of differentiation similar to that of the stoma illustrated in (D), after calcofluor staining. The ventral wall (arrow) fluoresces along its whole length. Scale bars: D = 1 μm; inset = 5 μm. (E, F) The median portion (E) of the ventral wall of the stoma shown in (D) and the junction of this wall with the external periclinal wall (F) at higher magnification. Note the membranous elements in the apoplast (small arrows). The arrowhead in (F) points to the middle lamella, while the large arrow points to the site of the future fore-chamber of the stomatal pore. EPW, external periclinal wall. Scale bars = 500 nm.

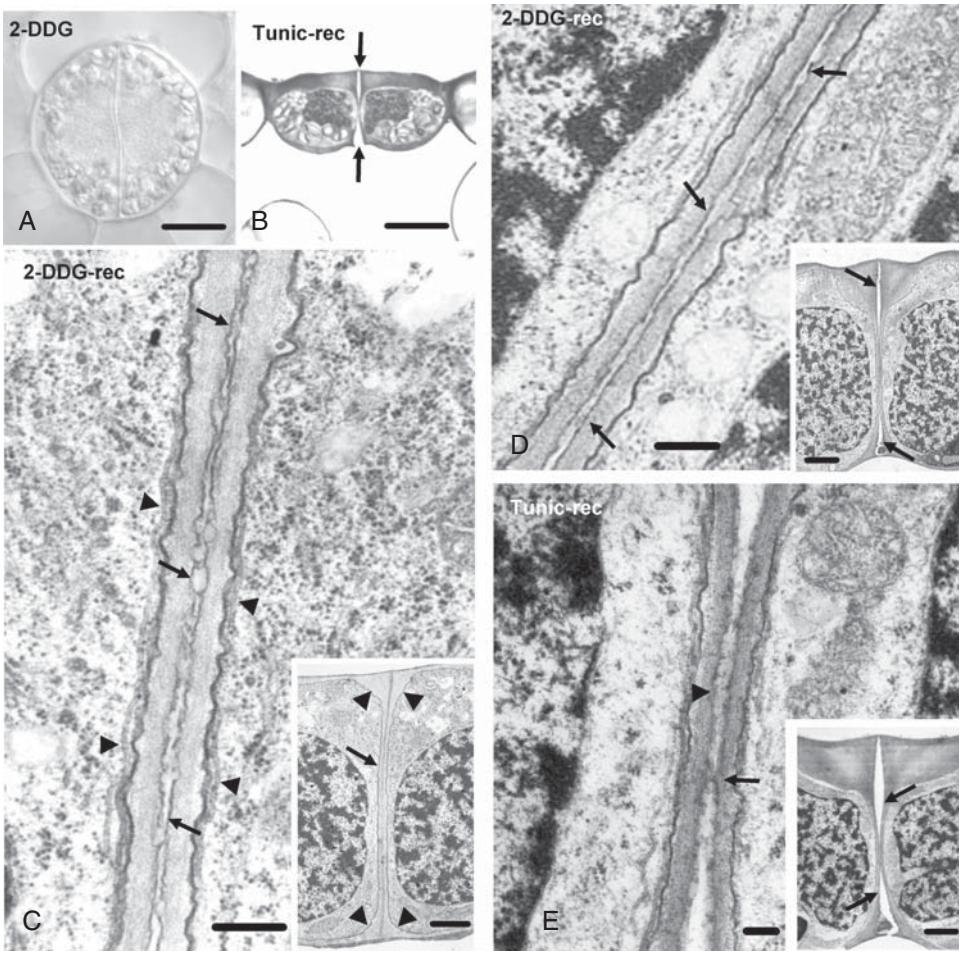

FIG. 8. (A) Differential interference contrast image of a 2-DDG-affected differentiating stoma. Treatment: 1 mM 2-DDG for 5 d. Scale bar = 10 μm. (B) Median transverse semi-thin section of a tunicamycin-affected stoma recovering under control conditions. This stoma, as well as those illustrated in (C–E), after treatment was placed in distilled water. The arrows point to the forming stomatal pore. Treatment: 12 μM tunicamycin for 5 d; recovery 7 d. Scale bar = 10 μm. (C) Higher magnification of a median transverse ventral wall section of a 2-DDG-affected stoma (inset), recovering under control conditions. The arrows in (C) mark the differentiated middle lamella, while the arrowheads mark microtubules. The arrow in the inset indicates the ventral wall and the arrowheads the wall thickenings. Treatment: 500 μM 2-DDG for 5 d; recovery 7 d. Scale bars: (C) = 250 nm; inset = 2·5 μm. (D) Median transverse ventral wall section of a 2-DDG-affected stoma (inset) recovering under control conditions. This stoma is at a more advanced stage of differentiation than that of the stoma shown in (C, inset). The fore- and rear-chamber of the stomatal pore have been formed (arrows in inset). The arrows in (D) mark the differentiated middle lamella. Treatment: 500 μM 2-DDG for 5 d; recovery 7 d. Scale bars: (D) = 250 nm; inset = 2·5 μm. (E) Median transverse ventral wall section of a tunicamycin-affected stoma (inset) recovering under control conditions, which is at a more advanced stage of differentiation than that of the stoma shown in (D, inset). The stomatal pore is at final stages of formation. The fore- and rear stomatal pore chambers (arrows in inset) have expanded towards the middle of the ventral wall. Note the material localized at the region of ventral walls that have not yet been separated (arrowhead in E). The arrow in (E) indicates a wall bridge connecting the adjacent ventral walls. Treatment: 12 μM tunicamycin for 5 d; recovery 7 d. Scale bars: (E) = 125 nm; inset = 2·5 μm.

oryzalin and colchicine disintegrated microtubules, inhibited stomatal pore formation and disturbed the pattern of GC wall thickenings (Apostolakos and Galatis, 1998; Zachariadis *et al.*, 1998). The differentiating oryzalin-affected stomata show atypical callose accumulations at various wall positions, including the aberrant wall thickenings (Fig. 10A; cf. Fig. 3F, H).

Cytochalasin B was also applied to determine whether actin filaments are involved in stomatal pore formation. Although treatment with 100 μM cytochalasin B for 48 h disintegrated the actin filaments in developing stomata (Apostolakos *et al.*, 2009), the pattern of callose deposition, at any stage of stomatal development, resembled that of control stomata (Fig. 10B; cf. Fig. 3F; see also Apostolakos *et al.*, 2009). However, in cytochalasin B-treated stomata internal stomatal pore formation was inhibited (Fig. 10C, D; cf. Fig. 5A, B). Microtubule organization was not affected in these stomata; well-organized anticlinal microtubule bundles lined the mid-region of their ventral wall (Fig. 10D).

CPA-treated stomata: disturbance of Ca^{2+} homeostasis inhibits callose deposition and stomatal pore formation

The post-cytokinetic and nascent ventral walls of CPA-affected stomata lacked callose, emitting weak callose fluorescence only at the sites of their junction with the periclinal and dorsal walls (Fig. 11A, B). Callose deposition in the developing wall thickenings of the affected stomata was also inhibited (Fig. 11C; cf. Fig. 3F). Only small callose

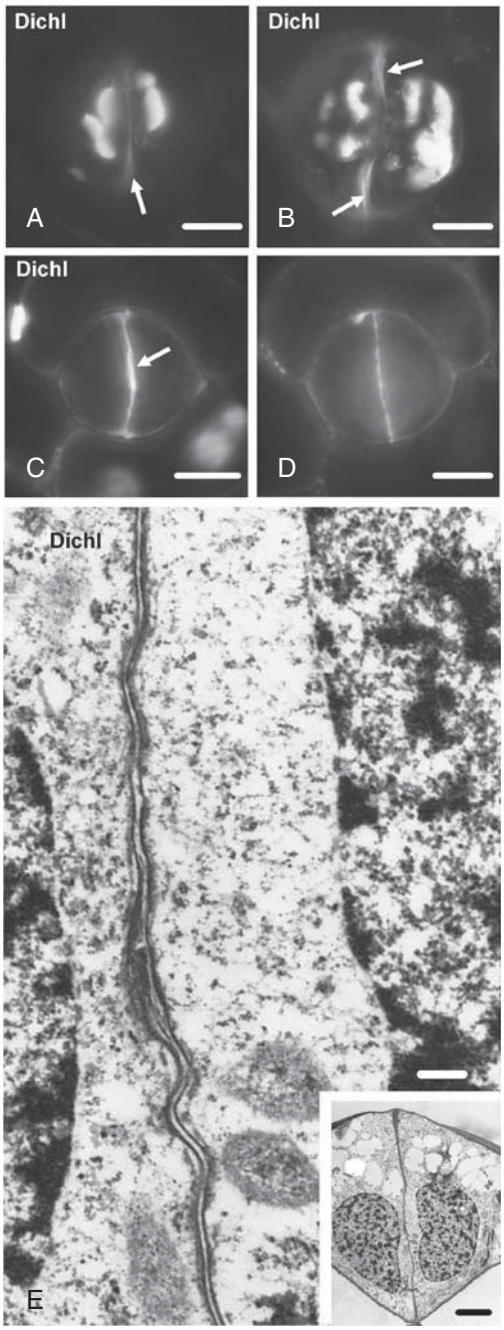

FIG. 9. Dichlobenil-affected stomata as they appear after aniline blue staining (A–D) or under TEM (E). Treatments: (A–E) 100 μM dichlobenil for 48 h. (A, B) Affected stomata at successive stages of differentiation. Atypical callose depositions can be seen at various sites of the periclinal walls. The arrows show regions of the ventral wall exhibiting autofluorescence (cf. Fig. 2B). Scale bars = 10 μm. (C, D) Optical sections through an external (C) and a median plane (D) of an affected stoma, which is at a stage of differentiation similar to that of the stoma shown in Fig. 3C and D. The external (C) and the median (D) region of the ventral wall emit intense callose fluorescence. The arrow in (C) indicates the initiating wall thickening at the junction of the ventral wall with the external periclinal wall. Scale bar = 10 μm. (E) Higher magnification of the median ventral wall region of the stoma shown in the inset. The internal stomatal pore has not been formed (cf. Fig. 5B). Inset: median transverse section of an affected stoma, which is at a stage of differentiation similar to that of the stomata shown in Fig. 5A and B. Note the absence of the wall thickenings at the sites of junction of the ventral wall with the periclinal walls (cf. Fig. 5B). Scale bars: (E) = 250 nm; inset = 5 μm.

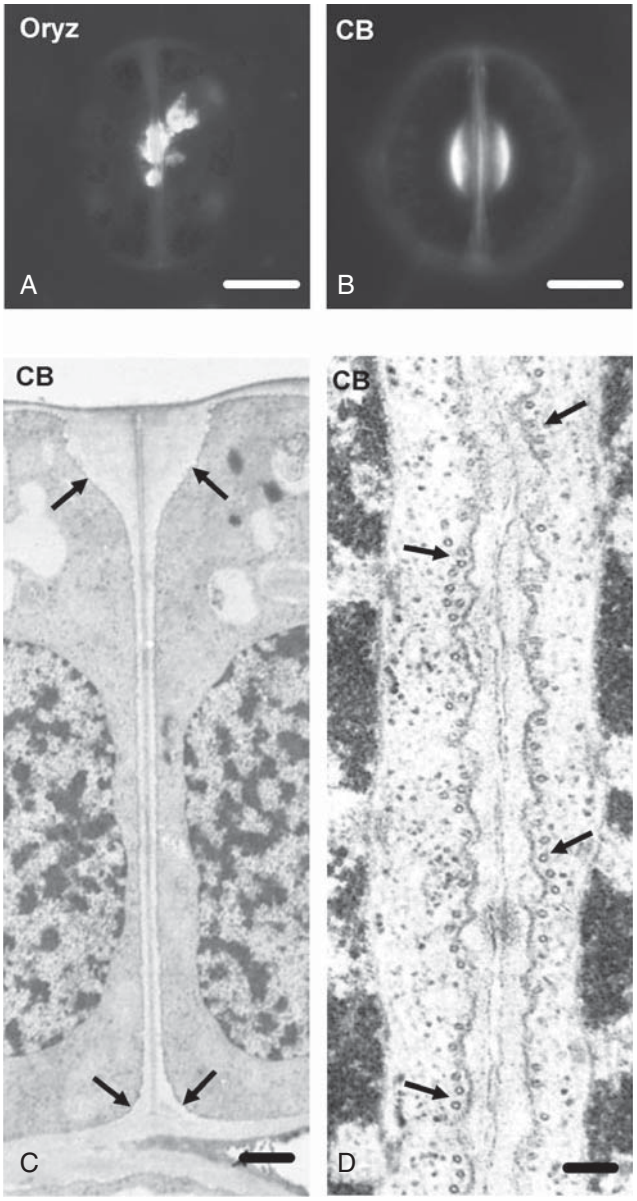

FIG. 10. Stomata treated with anti-cytoskeletal drugs as they appear after aniline blue staining (A, B) or under TEM (C, D). (A) Oryzalin-affected differentiating stoma exhibiting aberrant callose depositions at the stomatal pore region. The stage of differentiation of this stoma is similar to that of the stoma shown in Fig. 3F. Treatment: 50 μM oryzalin for 2 h. Scale bar = 10 μm. (B) Cytochalasin B-affected stoma, which is at a stage of differentiation similar to that of the stoma shown in Fig. 3F. The callose depositions at the stomatal pore region resemble those of the control stomata (cf. Figs 3F and 4A). Treatment: 100 μM cytochalasin B for 48 h. Scale bar = 10 μm. (C) Median transverse section of a cytochalasin B-affected stoma that is at a stage of differentiation similar to that of the stoma illustrated in Fig. 5B. The wall thickenings at the junctions of the ventral wall with the periclinal walls (arrows) do not differ from those of the untreated stomata. Stomatal pore formation has been inhibited (cf. Fig. 5B). Note the presence of the middle lamella along the ventral wall. Treatment: 100 μM cytochalasin B for 60 h. Scale bar = 1 μm. (D) Higher magnification of a median ventral wall region of a young cytochalasin B-affected stoma in paradermal view. Note the absence of the internal stomatal pore (cf. Fig. 5A). The arrows point to microtubules. Treatment: 100 μM cytochalasin B for 60 h. Scale bar = 125 nm.

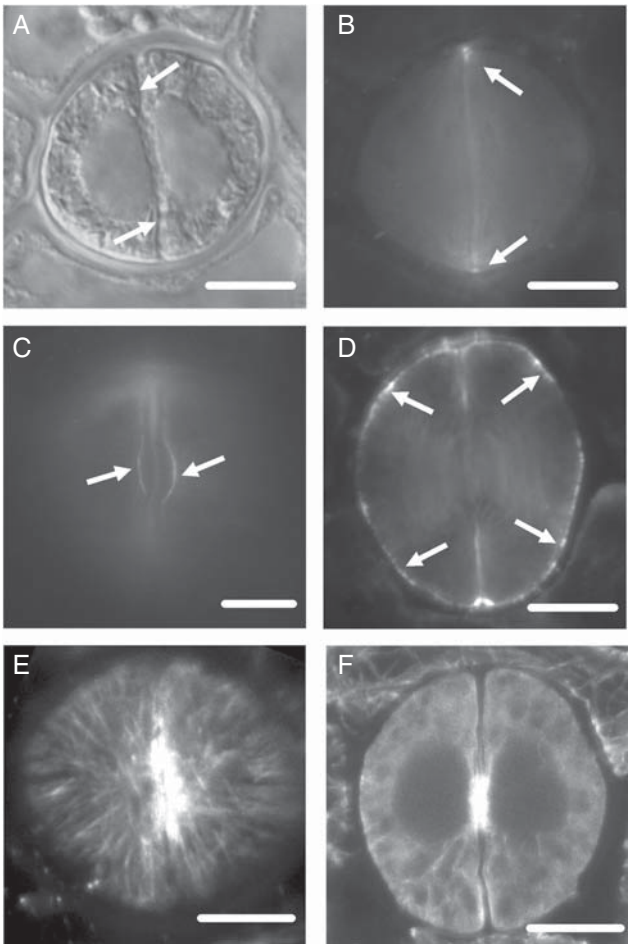

FIG. 11. CPA-affected stomata as they appear after callose (A–D) or microtubule (E, F) immunolocalization. Treatments: (A–F) 25 μM CPA for 24 h. (A) Differential interference contrast optical view of a post-cytokinetic affected stoma. (B) The stoma after callose immunolocalization. The nascent ventral wall (arrows in A) does not display callose fluorescence (B; cf. Figs 3B and 4A). Weak callose fluorescence is seen at the junction of the ventral wall with the dorsal walls (arrows in B). Scale bar = 10 μm. Optical sections through the external (C) and a median (D) plane of two affected stomata, which are at a differentiation stage similar to that of stomata shown in Fig 3F and H. Weak callose fluorescence is emitted by the stomatal pore region (arrows in C; cf. Fig. 3F, H) and by various positions of the dorsal walls (arrows in D). Scale bars = 10 μm. CLSM sections through the cortical cytoplasm below the external periclinal wall (E) and through a median plane (F) of an affected stoma at an early stage of differentiation, showing the microtubule organization. Scale bar = 10 μm.

accumulations in the periclinal and dorsal walls were visible (Fig. 11C, D).

Internal stomatal pore formation did not take place in the young affected stomata (Fig. 12A, B; cf. Fig. 5A, B), even though radial microtubule systems beneath the periclinal walls and anticlinal microtubule bundles along the mid-region of the ventral wall were present (Fig. 11E, F). In these stomata, the ventral wall in the stomatal pore region was thickened, enclosed membranous elements (Fig. 12B, C) and was positive to PAS staining (Fig. 12B, inset), indicating that it contained polysaccharides. Although in stomata treated at an advanced stage of differentiation the fore- and rear-pore chamber formation proceeded as in the untreated stomata (Fig. 12D; cf. Fig. 5C), the ventral walls did not separate in their median region (Fig. 12D, E; cf. Fig. 5C, D). As in the 2-DDG- or tunicamycin-affected stomata recovering in control conditions, lipophilic material was secreted along the middle lamella at this region (Fig. 12E; see also Supplementary Data Fig. S1B). Similar material has not been found in the same site of untreated stomata (Fig. 5D). The pattern of wall thickenings was not affected in CPA-treated stomata (Fig. 12D; cf. Fig. 5C), although the plasmalemma lining them formed outfoldings in the apoplastic space (Fig. 12F, small arrows). In Fig. 12F, a newly formed fore-chamber of the stomatal pore can be observed (large arrow), which is lined by cuticular material similar to that localized in the modified middle lamella of the ventral wall in Fig. 12E.

DISCUSSION

Callose and stomatal pore initiation

Stomatal pores are the exclusive passages for gaseous exchange between plants and the external environment, and thus an understanding of the mechanism of their formation is very important for plant cell biology. The present study has shown that callose is intimately involved in the 'internal opening' of the stomatal pore in *Asplenium nidus*, a process preceding the deposition of any detectable cell-wall material in the post-cytokinetic ventral wall (Apostolakos and Galatis, 1998, 1999). This conclusion is supported by the inhibition of internal stomatal pore formation with: (1) 2-DDG or tunicamycin, which inhibit callose synthesis; (2) CPA, a substance disturbing levels of cytoplasmic Ca^{2+} (Quader and Bechtler, 1996), which blocks callose formation in the affected stomata; and (3) coumarin or dichlobenil, which induce the deposition of larger quantities of callose in GCs and prolong callose presence in the nascent ventral walls. The data presented show that both inhibition and prolonged presence of callose in the nascent ventral wall inhibit internal stomatal pore formation.

In *A. nidus* stomata, the post-cytokinetic and nascent ventral walls possess abundant callose, probably offering mechanical support to the ventral wall plasmalemmata, as previously suggested (Samuels *et al.*, 1995; Hong *et al.*, 2001). The persistent callose probably delays the deposition of other cell-wall polysaccharides in nascent ventral wall, a phenomenon that might facilitate internal stomatal pore initiation via the cytoskeleton. The deposition of cell-wall materials before formation of the internal stomatal pore, followed by development of plasmalemma–cell-wall connections, would make local separation of the ventral wall plasmalemmata for internal stomatal pore formation difficult. The appearance of the nascent ventral wall in untreated stomata indicates that the deposition of cell-wall polysaccharides follows internal stomatal pore initiation (Apostolakos and Galatis, 1998).

Callose is maintained in the nascent ventral wall up to the organization of the anticlinal microtubule and actin filament bundles at the mid-region of the ventral wall (Apostolakos and Galatis, 1998, 1999). It then degrades locally and the cytoskeleton seems to mediate the separation of the adjacent plasmalemmata in this region. Callose degradation and internal stomatal pore formation commence at the centre of the ventral

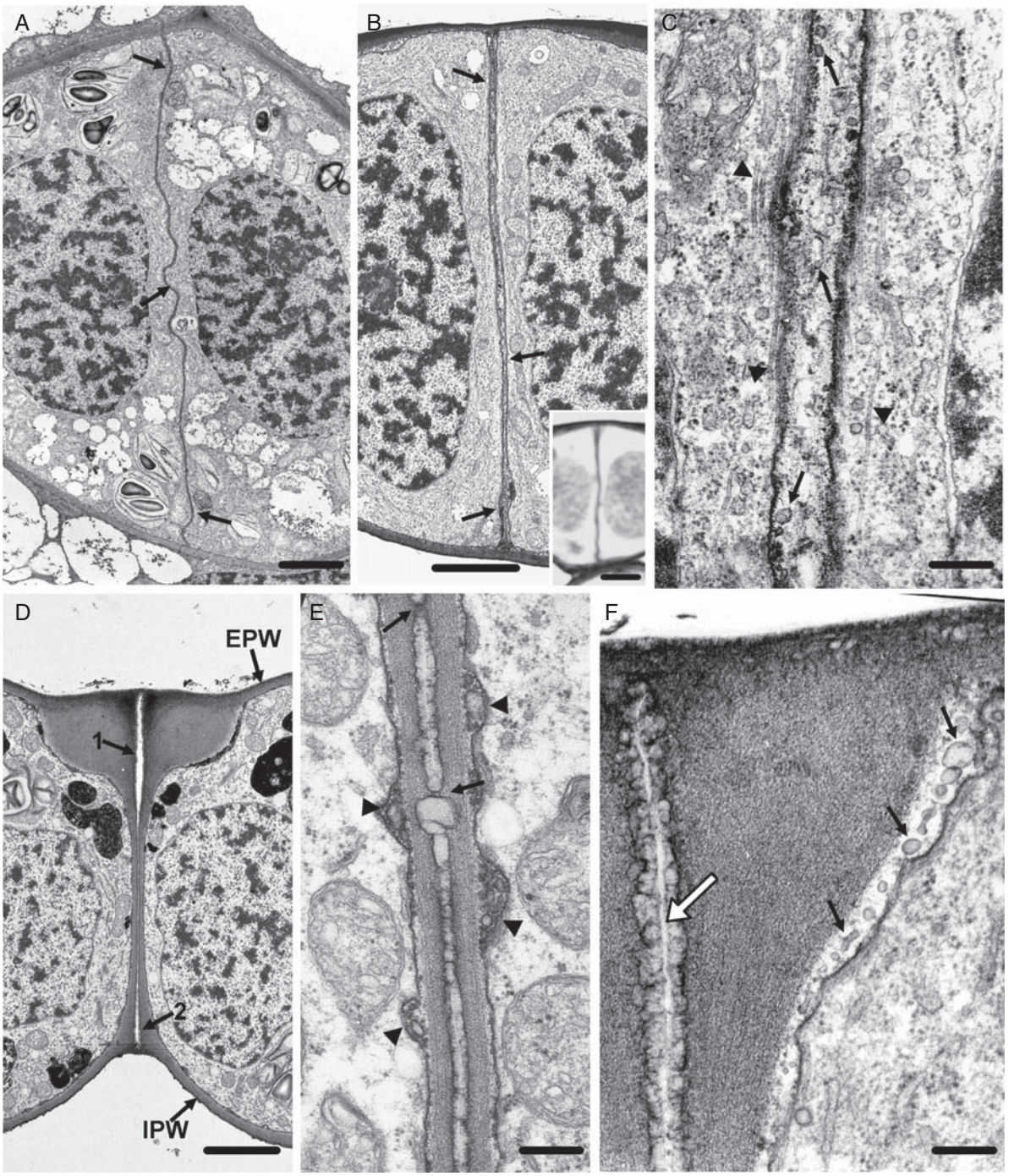

FIG. 12. TEM micrographs of CPA-affected stomata, in which internal stomatal pore formation has been inhibited. Treatments: (A–F) 25 μM CPA for 24 h. (A) Paradermal view through the middle of a post-cytokinetic affected stoma. The ventral wall (arrows) is wavy and lacks an internal stomatal pore (cf. Fig. 5A). Scale bar = 20 μm. (B) Median transverse section of an affected stoma at a stage of differentiation similar to that of the stoma depicted in Fig. 5B. The ventral wall (arrows) is atypically thickened and lacks an internal stomatal pore (cf. Fig. 5B). Inset: transverse semi-thin section of an affected stoma at a stage of differentiation similar to that of the stoma shown in (B), after PAS staining. The ventral wall and the periclinal walls are positively stained. Scale bars: (B) = 20 μm; inset = 5 μm. (C) Higher magnification of the median region of the ventral wall of the stoma shown in (B). The arrows show membranous elements at inner positions of the aberrant ventral wall and the arrowheads the microtubules. Scale bar = 250 nm. (D) Median transverse section of an affected stoma that is at a stage of differentiation more advanced than that of the stoma shown in (B). The arrows mark the initiating fore- (arrow 1) and rear- (arrow 2) chambers of the stomatal pore. EPW, external periclinal wall; IPW, internal periclinal wall. Treatment: 25 μM CPA for 24 h. Scale bar = 20 μm. (E) The median region of the ventral wall of the stoma shown in (D) at higher magnification. Note the absence of the internal stomatal pore (cf. Fig. 5C, D) and the material localized at the middle lamella. Wall bridges connect the adjacent ventral walls (arrows) and membranous elements are localized in the apoplast (arrowheads). Scale bar = 250 nm. (F) Wall thickening at the junction of the ventral wall with the external periclinal wall of a young affected stoma. The large arrow marks the initiated fore-pore chamber that is lined by a material similar to that localized in the middle lamella in (E). Note the membranous elements in the apoplast (small arrows). Scale bar = 250 nm.

wall and proceed towards its periphery. Therefore, the time and the mode of callose removal from the nascent ventral wall are accurately controlled in *A. nidus* stomata, probably establishing conditions favouring the formation of the internal stomatal pore. The pattern of callose deposition/degradation is controlled by local gradients of Ca^{2+}. The endoplasmic reticulum may be involved in the establishment of these gradients. The absence of callose in the CPA-affected nascent ventral walls (Fig. 11A, B) and the large quantities of endoplasmic reticulum in the cytoplasm lining them (Supplementary Data Fig. S2, available online) might support this hypothesis.

Treatments with 2-DDG, tunicamycin and CPA inhibited callose deposition in the post-cytokinetic ventral wall and blocked internal stomatal pore formation. The absence of callose probably allows the earlier deposition of wall materials that have a cohesive function in the aberrant ventral wall (see insets to Figs 7A and 12B), and also allow the development of connections between the ventral wall and the plasmalemmata, making internal stomatal pore formation impossible. The affected nascent ventral wall contains numerous membranous elements (Figs 7B, E and 12C), probably because of the extensive outfolding of the plasmalemma into the apoplast. Thus, the absence of callose seems to disturb not only the stability of the plasmalemma (see also van Amstel and Kengen, 1996), but also the balance of exocytotic/endocytotic membranous flow and the development of interconnections between the plasmalemma and the cytoskeletal elements. These phenomena could also affect the internal stomatal pore formation.

The cellulose synthesis inhibitors coumarin and dichlobenil blocked both internal stomatal pore formation and callose degradation in the nascent ventral wall. The presence of large quantities of callose in the cell wall, after inhibition of cellulose synthesis, has also been observed in other plants (Vaughn *et al.*, 1996; Sabba *et al.*, 1999). In the affected walls, the quantity of pectic materials increases considerably (Sabba *et al.*, 1999, and references therein). The persistent callose and the probable deposition of pectic materials in coumarin- or dichlobenil-affected ventral walls probably keep the plasmalemmata together, thereby preventing internal stomatal pore initiation. Moreover, both oryzalin and cytochalasin B inhibited internal stomatal pore initiation, disrupting the microtubule and actin filament cytoskeleton, respectively. A link between microtubules and internal stomatal pore formation has been previously described (Apostolakos and Galatis, 1998). That study also revealed that actin filaments are also involved in internal stomatal pore formation.

Alternative mechanism of stomatal pore formation in affected stomata

The inhibition of stomatal pore formation in 2-DDG- or tunicamycin-treated stomata is reversible. When the affected stomata where allowed to recover in distilled water, a stomatal pore was formed by the mechanism that commonly functions in plants (Fig. 1B, C; see review by Galatis and Apostolakos, 2004). In recovering stomata, the local detachment of the ventral wall begins from the external and the internal periclinal walls and proceeds inwards (Fig. 8B–E). A similar mechanism functions in CPA-affected stomata (Fig. 12D). Stomatal pore formation in most plants involves two processes: (1) weakening of the middle lamella of the ventral wall, and (2) application of mechanical forces that are generated during GC shaping, which disrupt the periclinal walls and separate the ventral wall partners of a GC pair at the stomatal pore site (Galatis and Apostolakos, 2004).

In the recovering and in the CPA-affected *A. nidus* stomata, these mechanical forces are generated as the GCs assume a kidney-like shape (see Figs 8A and 11D, F). The lipid material secreted in the middle lamella at the site of the future stomatal pore (Figs 8C, D and 12E; Supplementary Data Fig. S1) probably weakens the binding properties of the middle lamella, facilitating ventral wall separation, similar what has been reported for the stomata of the moss *Funaria hygrometrica* (Sack and Paollilo 1983; see also Sack, 1987) and those of the ferns *Polypodium vulgare* (Stevens and Martin, 1978) and *Azolla* spp. (Busby and Gunning, 1984). In the untreated *A. nidus* stomata, lipophilic material is secreted in the middle lamella of the polar ventral wall thickenings, probably facilitating broadening of the stomatal pore fore- and rear-chamber (Apostolakos and Galatis, 1999). Therefore, in *A. nidus* internal stomatal pore formation is not a prerequisite for stomatal pore formation. This species and probably all polypodiaceous ferns have developed an alternative mechanism to secure stomatal pore formation, if internal stomatal pore formation is inhibited.

Callose involvement in local wall thickening

This study confirmed previous observations (Apostolakos and Galatis, 1999) that significant quantities of callose are deposited in the newly formed local wall thickenings of *A. nidus* GCs. Matrix polysaccharides and cellulose microfibrils are then deposited. Gradually, callose is restricted to the margins of these thickenings, where cell-wall deposition continues. Callose was also localized in the aberrant wall thickenings of the oryzalin-affected GCs, a fact further suggesting that it plays a definite role in the local wall deposition.

Callose deposition is a general phenomenon in the developing cell-wall thickenings, as in stomata of other fern species (Peterson *et al.*, 1975; Peterson and Hambleton, 1978; Waterkeyn and Bienfait, 1979), in tracheary elements (Stone and Clarke, 1992; Gregory *et al.*, 2002), in transfer cells (Vaughn *et al.*, 2007), in cotton fibres (Waterkeyn, 1981; Salnikov *et al.*, 2003), in pollen tubes (Ferguson *et al.*, 1998), in moss spores (Schuette *et al.*, 2009) and in bordered-pits of tracheids (Chaffey and Barlow, 2002). In addition, callose is always present in the regenerating cell walls of protoplasts (van Amstel and Kengen, 1996; Sabba *et al.*, 1999). In GCs of *A. nidus* (present study) and of other fern species (Peterson *et al.*, 1975; Waterkeyn and Bienfait, 1979), callose is localized not only close to the plasmalemma but also to inner locations of wall thickenings, a phenomenon observed also in tracheary elements (Gregory *et al.*, 2002), pollen tubes (Ferguson *et al.*, 1998), moss spores (Schuette *et al.*, 2009) and cotton fibres (Salnikov *et al.*, 2003).

The role of callose in the deposition of GC wall thickenings is obscure (see also Peterson *et al.*, 1975; Waterkeyn and Bienfait, 1979). Callose may form gel-like matrices in the

cell wall, forming a suitable environment for the deposition of cellulose microfibrils and other wall polysaccharides (Waterkeyn, 1981; van Amstel and Kengen, 1996; Chaffey and Barlow, 2002; Salnikov *et al.*, 2003; Vaughn *et al.*, 2007). It has also been suggested that the degrading callose provides glucose residues for the synthesis of other cell-wall polysaccharides (Waterkeyn, 1981; Sabba *et al.*, 1999).

Alternatively, in *A. nidus* stomata callose deposition may also be triggered by some kind of 'wounding' or destabilization of the plasmalemma/cell-wall continuum during deposition of local wall thickenings. It is generally accepted that callose, among other functions, offers mechanical support to plasmalemma and/or the cell wall against stresses that are exerted on them (Parre and Geitmann, 2005; Vaughn *et al.*, 2007). The formation of extensive plasmalemma outfoldings into the apoplastic space in the atypical GC wall thickenings in stomata affected by callose synthesis inhibitors supports this hypothesis. Large quantities of callose are also deposited in the cell-wall thickenings of *A. nidus* stomata affected by cellulose synthesis inhibitors. The absence of cellulose, among others, probably makes these wall thickenings more sensitive to mechanical stresses, inducing in them the deposition of increased quantities of callose. Given the mechanical role that callose probably plays during cell plate growth (Samuels *et al.*, 1995; Vaughn *et al.*, 1996), it may also be suggested that this glucan might aid the progressive 'intrusion' of the GC wall thickenings into the cytoplasm (see also Vaughn *et al.*, 2007).

SUPPLEMENTARY DATA

Supplementary data are available online at www.aob.oxfordjournals.org and consist of the following figures. Fig. S1: Median transverse semi-thin sections of affected *Asplenium nidus* stomata stained with Sudan black B after treatment with 12 μM tunicamycin for 5 d then placed in distilled water for 7 d, and treatment with 25 μM CPA for 24 h. Fig. S2: Portion of the ventral wall of the stoma shown in Fig. 12A under higher magnification.

ACKNOWLEDGEMENTS

We are grateful to Dr H. Quader (Biocenter Klein Flottbek, University of Hamburg) and Dr E. Rigana (Biological Imaging Unit, Foundation of Biomedical Research, Athens) for access to their CLSM and TEM facilities. The present study was financed from the University of Athens (project 'Kapodistrias').

LITERATURE CITED

van Amstel TNM, Kengen HMP. 1996. Callose deposition in the primary wall of suspension cells and regenerating protoplasts, and its relationship to patterned cellulose synthesis. *Canadian Journal of Botany* **74**: 1040–1049.

Apostolakos P, Galatis B. 1998. Probable cytoskeleton involvement in stomatal pore formation in *Asplenium nidus* L. *Protoplasma* **203**: 48–57.

Apostolakos P, Galatis B. 1999. Microtubule and actin filament organization during stomatal morphogenesis in the fern *Asplenium nidus*. II. Guard cells. *New Phytologist* **141**: 209–223.

Apostolakos P, Livanos P, Galatis B. 2009. Microtubule involvement in the deposition of radial fibrillar callose arrays in stomata of the fern *Asplenium nidus* L. *Cell Motility and the Cytoskeleton* **66**: 342–349.

Bulone V. 2007. *In vitro* synthesis and analysis of plant (1 → 3)-β-D-glucans and cellulose: a key step towards the characterization of glucan synthases. In: Brown RM Jr, Saxena IM. eds. *Cellulose: molecular and structural biology*. Heidelberg: Springer, 123–145.

Busby CH, Gunning BES. 1984. Microtubules and morphogenesis in stomata of the water fern *Azolla*: an unusual mode of guard cell and pore development. *Protoplasma* **122**: 108–119.

Chaffey NJ, Barlow PW. 2002. Myosin, microtubules, and microfilaments: co-operation between cytoskeletal components during cambial cell division and secondary vascular differentiation in trees. *Planta* **214**: 526–536.

DeBolt S, Gutierrez R, Ehrhardt DW, *et al*. 2007. Morlin, an inhibitor of cortical microtubule dynamics and cellulose synthase movement. *Proceedings of the National Academy of Sciences, USA* **104**: 5855–5859.

Ferguson C, Teezi TT, Siika-aho M, Read SM, Bacic A. 1998. Location of cellulose and callose in pollen tubes and grains of *Nicotiana tabacum*. *Planta* **206**: 452–460.

Galatis B, Apostolakos P. 2004. The role of the cytoskeleton in the morphogenesis and function of stomatal complexes. *New Phytologist* **161**: 613–639.

Galatis B, Apostolakos P, Katsaros Ch. 1983. Microtubules and their organizing centres in differentiating guard cells of *Adiantum capillus-veneris*. *Protoplasma* **115**: 176–192.

Gregory ACE, Smith C, Kerry ME, Wheatley ER, Bolwell PG. 2002. Comparative subcellular immunolocalization of polypeptides associated with xylan and callose synthases in French bean (*Phaseolus vulgaris*) during secondary wall formation. *Phytochemistry* **59**: 249–259.

Hong Z, Delauney AJ, Verma DPS. 2001. A cell plate-specific callose synthase and its interaction with phragmoplastin. *Plant Cell* **13**: 755–768.

Jaffe MJ, Leopold AC. 1984. Callose deposition during gravitropism of *Zea mays* and *Pisum sativum* and its inhibition by 2-deoxy-D-glucose. *Planta* **161**: 20–26.

Meikle PJ, Bonig I, Hoogenraad MJ, Clarke AE, Stone BA. 1991. The location of (1–3)-beta-glucans in the walls of pollen tubes of *Nicotiana alata* using a (1–3)-beta-glucan-specific monoclonal antibody. *Planta* **185**: 1–8.

Montezinos D, Delmer DP. 1980. Characterization of inhibitors of cellulose synthesis in cotton fibers. *Planta* **148**: 305–311.

O'Brien TP, McCully ME. 1981. *The study of plant structure: principles and selected methods*. Melbourne: Termarcarphi Pty Ltd.

Panteris E, Apostolakos P, Galatis B. 2006. Cytoskeletal asymmetry in *Zea mays* subsidiary cell mother cells: a monopolar prophase microtubule half-spindle anchors the nucleus in its polar position. *Cell Motility and the Cytoskeleton* **63**: 696–709.

Panteris E, Galatis B, Quader H, Apostolakos P. 2007. Cortical actin filament organization in developing and functioning stomatal complexes of *Zea mays* and *Triticum turgidum*. *Cell Motility and the Cytoskeleton* **64**: 531–548.

Parre E, Geitmann A. 2005. More than a leak sealant. The mechanical properties of callose in pollen tubes. *Plant Physiology* **137**: 274–286.

Peterson RL, Hambleton S. 1978. Guard cell ontogeny in leaf stomata of the fern *Ophioglossum petiolatum*. *Canadian Journal of Botany* **56**: 2836–2852.

Peterson RL, Firminger MS, Dobrindt LA. 1975. Nature of the guard cell wall in leaf stomata of three *Ophioglossum* species. *Canadian Journal of Botany* **53**: 1698–1711.

Quader H. 1984. Tunicamycin prevents cellulose microfibril formation in *Oocystis solitaria*. *Plant Physiology* **75**: 534–538.

Quader H, Bechtler Ch. 1996. The calcium transport inhibitor cyclopiazonic acid reversibly affects the shape of the endoplasmic reticulum in onion epidermal cells. *Mitteilungen aus dem Institut fur Allgemeine Botanik Hamburg* **26**: 191–199.

Roland J-C. 1978. General preparation and staining of thin sections. In: Hall JL. ed. *Electron microscopy and cytochemistry of plant cells*. Amsterdam: Elsevier/North-Holland Biomedical Press, 1–62.

Sabba RP, Durso NA, Vaughn KC. 1999. Structural and immunocytochemical characterization of the walls of dichlobenil-habituated BY-2 tobacco cells. *International Journal of Plant Science* **160**: 275–290.

Sack FD. 1987. The development and structure of stomata. In: Zeiger E, Farquhar GD, Cowan IR. eds. *Stomatal function*. Stanford, CA: Stanford University Press, 59–89.

Sack FD, Paolillo DJ Jr. 1983. Stomatal pore and cuticle formation in *Funaria*. *Protoplasma* **116**: 1–13.

Salnikov V, Grimson MJ, Seagull RW, Haigler CH. 2003. Localization of sucrose synthase and callose in freeze-substituted secondary-wall-stage cotton fibers. *Protoplasma* **221**: 175–184.

Samuels AL, Giddings TH, Staehelin LA. 1995. Cytokinesis in tobacco BY-2 and root tip cells: a new model of cell plate formation in higher plants. *Journal of Cell Biology* **130**: 1345–1357.

Schuette S, Wood AJ, Geisler M, Geisler-Lee J, Ligrone R, Renzaglia KS. 2009. Novel localization of callose in spores of *Physcomitrella patens* and phylogenomics of the callose synthase gene family. *Annals of Botany* **103**: 749–756.

Škalamera D, Heath MC. 1996. Cellular mechanisms of callose deposition in response to fungal infection or chemical damage. *Canadian Journal of Botany* **74**: 1236–1242.

Stevens RA, Martin ES. 1978. Structural and functional aspects of stomata: I. Developmental studies in *Polypodium vulgare*. *Planta* **142**: 307–316.

Stone BA, Clarke AE. 1992. *Chemistry and biology of (1,3)-β-glucans*. Bundoora Australia: La Trobe University Press.

Vaughn KC, Hoffman JC, Hahn MG, Staehelin LA. 1996. The herbicide dichlobenil disrupts cell plate formation: immunogold characterization. *Protoplasma* **194**: 117–132.

Vaughn KC, Talbot MJ, Offler CE, McCurdy DW. 2007. Wall ingrowths in epidermal transfer cells of *Vicia faba* cotelydons are modified primary walls marked by localized accumulations of arabinogalactan proteins. *Plant & Cell Physiology* **48**: 159–168.

Verma DPS, Hong Z. 2001. Plant callose synthase complexes. *Plant Molecular Biology* **47**: 693–701.

Waterkeyn L. 1981. Cytochemical localization and function of the 3-linked glucan callose in the developing cotton fibre cell wall. *Protoplasma* **106**: 49–67.

Waterkeyn L, Bienfait A. 1979. Production et dégradation de callose dans les stomates des fougères. *La Cellule* **73**: 83–97.

Willmer C, Fricker M. 1996. *Stomata*, 2nd edn. London: Chapman and Hall.

Zachariadis M, Apostolakos P, Galatis B. 1998. Morphogenesis of 'floating' stomata in the fern *Anemia mandioccana*. Stomatal pore formation. In: Tsekos I, Moustakas M. eds. *Progress in botanical research*. Dordrecht: Kluwer Academic Publishers, 615–618.